

ENTROPY “FLOOR” AND EFFERVESCENT HEATING OF INTRACLUSTER GAS

S. ROYCHOWDHURY¹, M. RUSZKOWSKI^{2,4}, B. B. NATH¹ AND MITCHELL C. BEGELMAN^{2,3}*Accepted for the Astrophysical Journal*

ABSTRACT

Recent X-ray observations of clusters of galaxies have shown that the entropy of the intracluster medium (ICM), even at radii as large as half the virial radius, is higher than that expected from gravitational processes alone. This is thought to be the result of nongravitational processes influencing the physical state of the ICM. In this paper, we investigate whether heating by central AGN can explain the distribution of excess entropy as a function of radius. The AGN are assumed to inject buoyant bubbles into the ICM, which heat the ambient medium by doing pdV work as they rise and expand. Several authors have suggested that this “effervescent heating” mechanism could allow the central regions of clusters to avoid the “cooling catastrophe”. Here we study the effect of effervescent heating at large radii. We find that the results are mainly sensitive to the total energy injected into the cluster. Our calculations show that such a heating mechanism is able to solve the entropy problem, provided that the total energy injected by AGN is roughly proportional to the cluster mass. The inferred correlation is consistent with a linear relation between the mass of the central black hole(s) and the mass of the cluster, which is reminiscent of the Magorrian relation between the black hole and bulge mass.

Subject headings: galaxies: clusters: general — galaxies: active — dark matter — X-rays: galaxies: clusters — intergalactic medium — cooling flows

1. INTRODUCTION

Recent X-ray observations of both rich and poor clusters of galaxies have shown that there are problems in understanding the temperature, gas density or, equivalently, the entropy profiles at large radii ($\sim 0.5r_{\text{vir}}$, where r_{vir} is the virial radius) (Ponman et al. 2003). The observed entropy at $0.1r_{200}$ and at r_{500} (where r_{200} and r_{500} correspond to radii within which the average overdensity is 200 and 500, respectively) is higher than that estimated from the purely gravitational interaction of gas with dark matter (Ponman et al. 2003 and references therein; see also Roychowdhury & Nath 2003). Earlier X-ray observations by Lloyd-Davies et al. (2000) had shown that entropy at $0.1r_{200}$ reached a “floor” for poor clusters and groups. However, recent results of Ponman et al. (2003) have shown that the observed entropy is higher than the gravitational expectations for all clusters with emission-weighted temperatures $\langle T \rangle$ in the range 1 – 10 keV. The entropy at the much larger radius of r_{500} is also found to be higher than expected from purely gravitational processes.

Many theoretical models have been proposed to explain this phenomenon, including models that involve heat input from supernovae (Valageas & Silk 1999; Wu, Nulsen & Fabian 2000), gas cooling (Bryan 2000; Voit & Bryan 2001; Muanwong et al. 2002; Wu & Xue 2002; Davé, Katz & Weinberg 2002; Tornatore et al. 2003), accretion shocks (Tozzi & Norman 2001; Babul et al. 2002) and quasar outflows (Nath & Roychowdhury 2002).

Observations have also revealed the presence of X-ray deficient bubbles in the inner regions of many cooling flow clusters, e.g., the Hydra A cluster (McNamara et al. 2000), Abell 2052 (Blanton et al. 2001, 2003), Abell 2597 (McNa-

mara et al. 2001), Abell 4059 (Heinz et al. 2002), Abell 2199 (Johnstone et al. 2002), and others. These bubbles are characterized by low X-ray emissivity, implying low density compared to the ambient medium. In most of these cases, the cavities are clearly coincident with the radio lobes of the AGN in the cluster center. However, some clusters also exhibit cavities with weak or undetectable radio emission (known as “ghost bubbles” or “ghost cavities”) located far away from the cluster centers, like Perseus (Fabian et al. 2000), MKW3s (Mazzotta et al. 2002), and Abell 2597 (McNamara et al. 2001). These bubbles are also believed to be filled with relativistic plasma or buoyant gas deposited by jets from the central AGN, and are thought to rise through the ICM subsonically due to buoyancy. As they rise, radiative and adiabatic losses reduce the energy of the relativistic plasma inside the bubbles, resulting in a very low radio flux. The discovery of these bubbles and their detailed observational study have stimulated theoretical studies of the impact of these bubbles on the intracluster medium.

The evolution of these bubbles has been studied extensively in connection with the cooling flow catastrophe in the centers of clusters. It has been found recently that simple cooling flow model of clusters, which predict that the temperature of gas in the central regions of clusters should be very low (much less than 1 keV), are mostly in conflict with the observed temperature profiles (Peterson et al. 2001; Allen et al. 2001 and many others). Several authors have addressed whether the absence of very cold gas (below ~ 1 keV) can be explained by AGN energy input via outflows and bubbles (see, e.g., Tabor & Binney 1993, Binney & Tabor 1995, Ruszkowski & Begelman 2002, Churazov et al. 2002, Kaiser & Binney 2003, and Brüggén 2003a

¹ Raman Research Institute, Sadashivanagar, Bangalore -560080, India; suparna,biman@rri.res.in

² JILA, Campus Box 440, University of Colorado at Boulder, CO 80309-0440; mr@quixote.colorado.edu, mitch@jila.colorado.edu

³ Department of Astrophysical and Planetary Sciences, University of Colorado at Boulder

⁴ *Chandra* Fellow

for semi-analytic models; and Quilis et al. 2001, Reynolds et al. 2002, Brüggen 2003b, and Ruszkowski, Brüggen & Begelman 2004, Basson & Alexander 2003, Omma et al. 2003a, Omma & Binney 2003b for numerical simulations).

In this paper, we explore the possibility of heating the intracluster gas at large radii via the “effervescent heating” mechanism (Begelman 2001, Ruszkowski & Begelman 2002). Since the excess entropy requirements at different radii are different, the questions we set out to answer are the following:

1. Is it possible to satisfy simultaneously the entropy observations at two fiducial radii ($0.1r_{200}$ and r_{500}) with a single central heating source for all clusters? We explore the parameter space of time-averaged jet luminosity $\langle L \rangle$ and the time for which this activity continues, t_{heat} .
2. How does the entropy profile of the cluster gas evolve with time when it is being heated and cooled simultaneously?

The paper is organized as follows. In § 2 we describe our model, including initial conditions, details of the effervescent heating mechanism, our prescriptions for cooling and convection, and the simulation method. The results and discussion are presented in §§ 3 and 4, respectively. We discuss caveats of our model in § 5 and summarize our conclusions in § 6.

2. MODEL

Our model of the ICM assumes that the thermal gas remains in hydrostatic equilibrium as it is heated by buoyant radio bubbles, originating from the central AGN, via the “effervescent heating” mechanism. Here, we begin with a description of the background dark matter potential of the cluster.

2.1. Dark matter density profile

We assume that the dark matter density profile of the cluster, $\rho_{\text{dm}}(r)$, is described by a self-similar form as suggested by many high resolution N -body simulations. The profile is expressed in terms of a characteristic radius, r_s , by

$$\rho_{\text{dm}}(r) = \frac{\rho_s}{x(1+x)^2} \quad (1)$$

(see, e.g., Komatsu & Seljak 2002), where ρ_s is a characteristic density and $x = r/r_s$. We define a dimensionless “concentration parameter” $c \equiv r_{\text{vir}}/r_s$, where the virial radius r_{vir} is calculated from the spherical collapse model (Peebles 1980) assuming overdensity $\Delta_c(z=0) = 100$ (Komatsu & Seljak 2002). The characteristic density ρ_s is then given by

$$\rho_s = c^3 \frac{M_{\text{vir}}}{4\pi r_{\text{vir}}^3} \left[\ln(1+c) - \frac{c}{(1+c)} \right]^{-1}, \quad (2)$$

where M_{vir} is the cluster virial mass. The concentration parameter c can be approximated by

$$c = 9 \left(\frac{M_{\text{vir}}}{1.5 \times 10^{13} h^{-1} M_\odot} \right)^{-0.13}, \quad (3)$$

according to numerical simulations by Bullock et al. (2001) (we use $h = 0.71$).

The above set of equations specifies the dark matter density profile of a particular cluster as a function of its virial mass. Next, we turn our attention to the density profile of the gas in hydrostatic equilibrium with this dark matter distribution.

To compare our results with observations, we present our results in terms of the radii r_{200} and r_{500} , where the overdensities are 200 and 500, respectively. Both radii are functions of the cluster mass. The ratio $r_{500}/r_{200} \approx 0.65 - 0.67$ for the range of masses we have considered.

2.2. Initial configuration of intracluster gas

We use the “universal temperature profile” (Loken et al. 2002) as the initial temperature profile of gas in hydrostatic equilibrium to determine the initial density profile. This profile is different from the commonly used self-similar profile, which assumes that the intracluster gas density distribution scales as the dark matter density profile with a constant of proportionality $f_b = \frac{\Omega_b}{\Omega_m}$ (i.e., $\rho_{\text{gas}} = f_b \rho_{\text{dm}}$). We use the “universal temperature profile” instead of the self-similar profile because the former is claimed to be the result of gravitational processes alone. Moreover, it does not have the unrealistic turnover of the temperature profile in the inner regions of the cluster, which one finds in the self-similar profile (Roychowdhury & Nath 2003).

The initial temperature profile (normalized by the emission-weighted temperature $\langle T \rangle$), in the radial range $0.04r_{\text{vir}} \leq r \leq r_{\text{vir}}$, is given by

$$\frac{T_o(r)}{\langle T \rangle} = \frac{b}{(1+r/a)^\delta} \quad (4)$$

where $b = 1.33$, $a = r_{\text{vir}}/1.5$, and $\delta = 1.6$. To determine the emission-weighted temperature from the cluster mass, we use a relation that arises from adiabatic evolution of the gas in the cluster. Afshordi & Cen (2002) have shown that the observations by Finoguenov et al. (2001) of the $M_{500}-\langle T \rangle$ relation in clusters can be understood from gravitational processes alone. We therefore use this empirical relation ($M_{500}-\langle T \rangle$) derived by Finoguenov et al. (2001):

$$M_{500} = 2.64 \times 10^{13} \left(\frac{k_b \langle T \rangle}{1 \text{ keV}} \right)^{1.78} M_\odot, \quad (5)$$

where k_b is the Boltzmann constant and M_{500} has been calculated self-consistently by taking the total mass within the radius where the over-density is $\delta \geq 500$.

The equation of hydrostatic equilibrium for gas in a cluster with temperature $T_o(r)$ and density $\rho_{\text{gas}}(r)$ is

$$\frac{1}{\rho_{\text{gas}}(r)} \frac{d}{dr} (P_{\text{gas}}(r)) = -\frac{GM(\leq r)}{r^2}, \quad (6)$$

where $P_{\text{gas}} = (\rho_{\text{gas}}/\mu m_p) k_b T_o$, $M(\leq r)$ is the total mass inside radius r , and μ and m_p denote the mean molecular weight ($\mu = 0.59$) and the proton mass, respectively. The boundary condition imposed on the solution is that the gas-fraction, $f_{\text{gas}} \equiv M_{\text{gas}}/M_{\text{dm}} = 0.13333$, within r_{200} is universal, as recently found by Ettori (2003) for a sample of low- and high-redshift clusters.

2.3. Heating, cooling and convection

2.3.1. Heating

In the “effervescent heating” model, the central AGN is assumed to inflate buoyant bubbles of relativistic plasma in the ICM (Begelman 2001, Ruszkowski & Begelman 2002). The timescale for the bubbles to cross the cluster (of order the free-fall time) is shorter than the cooling timescale. Since the number flux of bubbles is large, the flux of bubble energy through the ICM approaches a steady state. This implies that details of the energy injection process such as the number flux of bubbles, the bubble radius or size, filling factor and rate of rise do not affect the average heating rate.

It is assumed that the relativistic gas does not mix with the ICM very efficiently. Under such conditions the bubbles can expand and do $p dV$ work on the ambient medium as they rise in the cluster pressure gradient. We assume that this work converts internal energy of the bubbles to thermal energy of the intracluster gas within a pressure scale height of where it is generated. Then, in a steady state (and assuming spherical symmetry), the energy flux carried by the bubbles varies as

$$F_b \propto \frac{P_b(r)^{(\gamma_b-1)/\gamma_b}}{r^2} \quad (7)$$

where $P_b(r)$ is the partial pressure of buoyant gas inside the bubbles at radius r and γ_b is the adiabatic index of buoyant gas, which we have taken to be $4/3$. This formula includes the effects of adiabatic bubble inflation. Assuming that the partial pressure inside these bubbles scales as the thermal pressure of the ICM, the volume heating function \mathcal{H} can be expressed as

$$\begin{aligned} \mathcal{H} &\sim -r^2 h(r) \nabla \cdot (\hat{\mathbf{r}} F_b) \\ &= -h(r) \left(\frac{P_{\text{gas}}}{P_0} \right)^{(\gamma_b-1)/\gamma_b} \frac{1}{r} \frac{d \ln P_{\text{gas}}}{d \ln r}, \end{aligned} \quad (8)$$

where P_0 is some reference pressure and $h(r)$ is the normalization function

$$h(r) = \frac{\langle L \rangle}{4\pi r^2} (1 - \exp(-r/r_0)) q^{-1}. \quad (9)$$

In equation (9), $\langle L \rangle$ is the time-averaged energy injection rate and r_0 is the inner heating cut-off radius which is determined by the size of the central heating source. In our calculations r_0 is taken to be $0.01 r_{\text{vir}}$, which is $\sim 15 - 20$ kpc depending on the cluster mass $M_{\text{cl}} (\equiv M_{\text{vir}})$. The normalization factor q is defined by

$$q = \int_{r_{\text{min}}}^{r_{\text{max}}} \left(\frac{P}{P_0} \right)^{(\gamma_b-1)/\gamma_b} \frac{1}{r} \frac{d \ln P}{d \ln r} (1 - e^{-r/r_0}) dr, \quad (10)$$

where $r_{\text{max}} = r_{200}$.

2.3.2. Cooling and convection

To calculate the volume cooling rate, we use a fit to the normalized cooling function $\Lambda_{\text{N}}(T)$ for a metallicity of $Z/Z_{\odot} = 0.3$, as calculated by Sutherland & Dopita (1993). This cooling function incorporates the effects of free-free emission and line cooling. The fit is borrowed from Nath

(2003). Thus, the volume cooling rate is $\Gamma = n_e^2 \Lambda_{\text{N}}(T)$, where $n_e = 0.875(\rho/m_p)$ is the electron density.

The convective flux F_{conv} is given by the mixing length theory,

$$F_{\text{conv}} = \begin{cases} 2^{-5/2} c_p^{-1/2} T g^{1/2} \rho_{\text{gas}} l_m^2 (-\nabla \hat{s})^{3/2} & \text{if } \nabla \hat{s} < 0, \\ 0 & \text{otherwise,} \end{cases} \quad (11)$$

where g is the gravitational acceleration, l_m is the mixing length, $\hat{s} = (\gamma - 1)^{-1} k_b / (\mu m_p) \ln(P_{\text{gas}}/\rho_{\text{gas}}^{\gamma})$ is the gas entropy per unit mass, and $c_p = \gamma k_b / [(\gamma - 1)\mu m_p]$ is the specific heat per unit mass at constant pressure. We use $l_m = \min[0.3 P_{\text{gas}} / (\rho_{\text{gas}} g), r]$, where r is the distance from the cluster center.

2.3.3. Evolution of the intracluster gas

As noted earlier, the gas is assumed to be in quasi-hydrostatic equilibrium at all times since the cooling is not precipitous at these radii and the heating is mild. The gas entropy per particle is

$$S = \text{const} + \frac{1}{\gamma - 1} k_b \ln(\sigma). \quad (12)$$

where $\sigma \equiv P_{\text{gas}}/\rho_{\text{gas}}^{\gamma}$ is the “entropy index” and γ is the adiabatic index. The particle number density of the gas, n , is given by $n = \rho_{\text{gas}}/\mu m_p$.

During each timestep Δt , the entropy of a given mass shell changes by an amount

$$\Delta S = \frac{1}{\gamma - 1} k_b \frac{\Delta \sigma}{\sigma} = \frac{1}{nT} (\mathcal{H} - \Gamma - \nabla \cdot F_{\text{conv}}) \Delta t. \quad (13)$$

Incorporating the expressions for heating, cooling, and convection, the entropy increment for each mass shell for a timestep Δt becomes

$$\begin{aligned} \Delta \sigma(M) &= \frac{2}{3} \frac{\sigma}{P_{\text{gas}}} \Delta t \left[-h(r) \left(\frac{P_{\text{gas}}}{P_0} \right)^{(\gamma_b-1)/\gamma_b} \right. \\ &\quad \times \left. \frac{1}{r} \frac{d \ln P_{\text{gas}}}{d \ln r} - n_e^2 \Lambda_{\text{N}}(T) \right. \\ &\quad \left. - \frac{1}{r^2} \frac{d}{dr} (r^2 F_{\text{conv}}) \right] \end{aligned} \quad (14)$$

where n_e and P_{gas} are the current electron number density and pressure of the ICM, respectively.

Thus, the entropy index of each mass shell of gas due to heating and cooling after a time Δt becomes

$$\sigma_{\text{new}}(M) = \sigma_0(M) + \Delta \sigma(M) \quad (15)$$

where $\sigma_0(M) = P_{\text{gas0}}/\rho_{\text{gas0}}^{\gamma}$ is the default entropy index. The system relaxes to a new state of hydrostatic equilibrium with a new density and temperature profile. After updating the function $\sigma(M)$ for each mass shell, we solve the equations

$$\frac{dP_{\text{gas}}}{dM} = \frac{GM(\leq r)}{4\pi r^4} \quad (16)$$

$$\frac{dr}{dM} = \frac{1}{4\pi r^2} \left(\frac{P_{\text{gas}}(M)}{\sigma(M)} \right)^{(1/\gamma)} \quad (17)$$

to determine the new density and temperature profiles at time $t + \Delta t$. The boundary conditions imposed on these equations are that (1) the pressure at the boundary of the

cluster, r_{out} , is constant and is equal to the initial pressure at r_{200} , i.e., $P(r_{\text{out}}) = \text{constant} = P_{\text{gas0}}(r_{200})$, and (2) the gas mass within r_{out} at all times is the mass contained within r_{200} for the default profile at the initial time, i.e., $M_{\text{g}}(r_{\text{out}}) = M_{\text{g0}}(r_{200}) = 0.1333M_{\text{dm}}(r_{200})$. It is important to note here that r_{out} increases as the cluster gas gets heated and spreads out.

The observed gas entropy $\mathcal{S}(r)$ at $0.1r_{200}$ and at r_{500} is then calculated using

$$\mathcal{S}(r) \equiv T(r)/n_{\text{e}}^{2/3}(r). \quad (18)$$

The updated values of $\sigma(M)$ and pressure of the ICM $P_{\text{gas}}(r)$ are used to calculate the heating and cooling rates and the convective flux for the next time step. This is continued for a duration of t_{heat} . After that the heating source is switched off, putting $\mathcal{H} = 0$. The cooling rate and convective flux continue to be calculated to update the function $\sigma(M)$ at subsequent timesteps, and the hydrostatic structure is correspondingly evolved for a duration of $t_{\text{H}} - t_{\text{heat}}$, where t_{H} is the Hubble time. Note that r_{out} decreases during this time since the intracluster gas loses entropy and shrinks. The only free parameters in our calculation are the energy injection rate $\langle L \rangle$ and the time t_{heat} over which the ‘‘effervescent heating’’ of the ICM takes place. After evolving the gas for the total available time, $t_{\text{H}} \sim 1.35 \times 10^{10}$ years, we check whether the entropy at $0.1r_{200}$ and r_{500} matches the observed values, and adjust parameters accordingly. In this way, we explore the parameter space of $\langle L \rangle$ and t_{heat} for different cluster masses so that the entropy (after 1.35×10^{10} years) at $0.1r_{200}$ and r_{500} matches the observed values.

For numerical stability of the code, the convection term is integrated using timesteps that satisfy the appropriate Courant condition. The Courant condition for convection is

$$\Delta t_{\text{conv}} \leq \frac{1}{2} 2^{5/2} \sqrt{\gamma} \frac{(\Delta r)^{5/2}}{g^{1/2} l_{\text{m}}^2}. \quad (19)$$

The timesteps, Δt , used in equation (14) to update the entropy of the gas and calculate its pressure, temperature and density profiles always obey the above Courant condition (Ruszkowski & Begelman 2002; Stone, Pringle & Begelman 1999).

The calculations presented in this paper were also performed using the fully time-dependent *ZEUS* code (Clarke, Norman & Fiedler 1994) and the results obtained were consistent with the ones presented here. However, we decided to use our quasi-hydrostatic Lagrangian code as it allowed us to search the parameter space more efficiently.

3. RESULTS

In this section, we discuss our results for cluster evolution due to heating, cooling and convection. The gas is heated for a time t_{heat} and cooled simultaneously. After this time, the heating source is switched off. The gas is then allowed to cool radiatively until a total simulation time of $t_{\text{H}} = 1.35 \times 10^{10}$ years has elapsed. The final entropy values at $0.1r_{200}$ and r_{500} are compared with the observed ones.

In Figure 1, the observed entropy values and their errors at $0.1r_{200}$ and at r_{500} are plotted as a function of the

emission-weighted temperature, $\langle T \rangle$, of the cluster (Ponman et al. 2003). We have done a best-fit analysis on these data points to estimate the entropy requirements for the sample of clusters of masses ranging from 10^{14} to $2 \times 10^{15} M_{\odot}$. The results of our analysis are the shaded regions in the two panels of Figure 1. The solid line through the center of the shaded region is the best-fit curve with the lines bounding the shaded region being the $1 - \sigma$ errors on the best-fit entropy values.

Figure 2 shows the time evolution of scaled entropy profiles of a cluster of mass $M_{\text{cl}} = 6 \times 10^{14} M_{\odot}$ with and without convection for $\langle L \rangle = 3 \times 10^{45} \text{ erg s}^{-1}$. We use the same method of emissivity weighting as in Roychowdhury & Nath (2003) to calculate the average quantities. The entropy profiles are plotted in time-steps of 5×10^8 years. They are seen to rise with time as the ICM is heated. Then, after the heating is switched off (after $t_{\text{heat}} = 5 \times 10^9$ years), the gas loses entropy due to cooling and the profiles are seen to fall progressively until the Hubble time is reached. The inclusion of convection flattens the negative gradient in the scaled entropy profiles in the central regions of the cluster (within $0.2r_{200}$, as seen in the difference of the entropy profiles between the left and right panels in Figure 2. The plot that includes convection (left panel in Figure 2) shows that the gas develops a flat entropy core in its central regions after the heating source has been switched off and the gas has cooled.

Figure 3 shows the evolution of density and temperature of the ICM for a cluster of mass $6 \times 10^{14} M_{\odot}$ and for a luminosity of $\langle L \rangle = 3 \times 10^{45} \text{ erg s}^{-1}$. The gas density decreases with time during the heating epoch, and increases due to radiative cooling and convection after the heating source is switched off. It is interesting to note that the changes in density are minimal beyond $0.2r_{200}$, and that convection plays an important role in regulating the density profiles after the heating source is switched off for radii $r \leq 0.2r_{200}$. We note that for clusters with lower emission-weighted temperatures, the effects of heating and convection are seen at larger radii.

We now discuss the permitted range in the total energy injected into the cluster, $E_{\text{agn}} = \langle L \rangle \times t_{\text{heat}}$, required to match the observed entropy as a function of the cluster mass. Figure 4 shows the spread in E_{agn} as a function of the cluster mass for two different values of t_{heat} . The region bounded by thin solid lines is the permitted range in energy for $t_{\text{heat}} = 5 \times 10^8$ years. This region includes an area shaded with solid vertical lines, which corresponds to the values of E_{agn} that satisfy the entropy requirement at $0.1r_{200}$, and another area shaded with solid oblique lines which satisfies the entropy requirement at r_{500} . Similarly, the region bounded by thin dotted lines in Figure 4a shows the permitted spread in energy for $t_{\text{heat}} = 5 \times 10^9$ years. This region includes an area shaded with dots which corresponds to the values of E_{agn} that satisfy the entropy requirement at $0.1r_{200}$ and another area shaded with long-dashed horizontal lines, which satisfies the entropy requirement at r_{500} . For cluster masses above $9 \times 10^{14} M_{\odot}$ there is no lower limit on the injected energy from the entropy measurements at r_{500} . The region corresponding to this situation is marked by horizontal dashed lines and oblique lines for cluster masses above $9 \times 10^{14} M_{\odot}$.

Figure 5 shows the permitted total injected energy range

as a function of the mass of cluster for heating times between $t_{\text{heat}} = 5 \times 10^8$ years and $t_{\text{heat}} = 5 \times 10^9$ years. Here the entropy is required to match observations at *both* $0.1r_{200}$ and r_{500} . The thick solid line represents a linear relation between the total energy injected to the cluster by AGN and the mass of the cluster (see next section for more details).

4. DISCUSSION

As is clear from Figures 4 and 5, it is possible to heat the ICM with a *single* central AGN to match the entropy requirements at *both* $0.1r_{200}$ and r_{500} . However, in order to match the entropy at both radii, the total injected energy E_{agn} , for a given value of $t_{\text{heat}} \ll t_{\text{H}}$, must be tightly constrained. In fact, our calculations have shown that for any value of $t_{\text{heat}} < t_{\text{H}}$, i.e., for any heating time (or AGN lifetime), it is always possible to satisfy the entropy observations at *both* radii with a *single* value of the luminosity $\langle L \rangle$. This is different from the cooling flow problem, where $\langle L \rangle$ must be finely tuned to match the cooling rate (Ruszkowski & Begelman 2002), because cooling effects on large scales are rather mild and, thus, the results depend mostly on the total injected energy $E_{\text{agn}} = \langle L \rangle \times t_{\text{heat}}$. Thus, if we can fit the observed entropy values for just one pair $\langle L \rangle$ and t_{heat} , we can do so for a wide range of such pairs. Another manifestation of this fact is that the plots in Figure 4 are similar in shape but are just offset by a factor of a few. As the cooling effects are relatively mild, the modest differences arise because shorter heating times lead to higher temperatures and convective transport cannot “catch up” with the energy supply. As the entropy excess to be explained is known from observations and is fixed, more heat has to be injected for shorter heating times. Nevertheless, the results are mostly sensitive to the *total* energy input from the black hole, rather than to $\langle L \rangle$ and t_{heat} separately. As a consequence, satisfactory fits can be obtained as long as the total injected energy falls within a relatively narrow range of values, which depends on the cluster mass (Figure 5).

As an illustrative example of such a relation, the thick solid line plotted in Figure 5 shows a linear relation between E_{agn} and cluster mass, M_{cl} , that is consistent with the requirements from entropy observations for a heating time of $5 \times 10^8 \leq t_{\text{heat}} \leq 5 \times 10^9$ years. We point out that the effective heating time may be longer than the integrated AGN lifetimes. Heating of the cluster may occur more gradually as heat gets distributed on a timescale very roughly proportional to the sound crossing time from the cluster center to a given radius. Thus, t_{heat} should be interpreted as an upper limit on the AGN lifetime.

Let us assume that the bulge mass of the central AGN is related by a factor f to the cluster mass as $M_{\text{h}} \sim f M_{\text{cl}}$ and that the mass of the black hole is related to the bulge mass of the AGN host by $M_{\text{bh}} \sim 1.5 \times 10^{-3} M_{\text{h}}$ (Häring & Rix 2004; Ferrarese & Merritt 2000, Gebhardt et al. 2000). This means that the mass of the black hole is related to the cluster mass by $M_{\text{bh}} \sim 1.5 \times 10^{-5} f_{-2} M_{\text{cl}}$, where $f_{-2} = f/0.01$. It is generally thought that AGN are fuelled by accretion onto the supermassive black hole. If we require that a fraction η of the mass of the black hole is converted into energy, then the relation between the black hole mass and the total injected energy becomes

$M_{\text{bh}} \sim 2.8 \times 10^8 \eta_{0.2}^{-1} E_{62} M_{\odot}$, where $\eta_{0.2} = \eta/0.2$. The relation between the total injected energy and the cluster mass is $E_{62} \sim 5.4 \eta_{0.2} f_{-2} M_{14}$. The linear relation in Figure 5 corresponds to $f_{-2} \eta_{0.2} = 0.25$.

Note that for longer heating times the luminosity constraints become less stringent and lower black hole masses can explain the observed trends. Finally, as we consider heating on large scales, all galaxies in the cluster that go through an active phase will contribute to the overall energy budget of the cluster gas. For example, substructure in the cluster could contain galaxies with sizable bulge components, each of which may contain a supermassive black hole. Therefore, the constraint on the black hole mass obtained above should be interpreted as a sum of all black hole masses that contribute to heating rather than the mass of an individual black hole. This could also lower the required efficiency of individual black holes that contribute to cluster heating.

Finally, we note that cooling and convection play important roles in controlling the heating mechanism so that the entropy profiles broadly match the observed entropy profiles in clusters (Ponman et al. 2003). Notably, in the later stages of evolution of the gas, after the heating source is switched off, convection flattens the entropy profiles in the central regions of the cluster. Moreover, an entropy core seems to develop in the final stages of the evolution of the ICM. This is consistent with the observed entropy profiles, which show cores at $r \leq 0.1r_{200}$ (Ponman et al. 2003). Our entropy profiles do not show steep positive gradients as observed in the entropy profiles of two groups of galaxies (Mushotzky et al. 2003). However, these groups have masses smaller than the ones considered here. Moreover, since the temperature profiles show a temperature gradient even though the entropy is flattened, thermal conduction might be able to conduct heat out from the central regions of the cluster and reduce temperatures there. This will happen at roughly constant pressure and, therefore, central densities will slightly increase. Thus conduction (if not fully suppressed) may help to remove the core in the center. Analyzing the effects of conduction is not within the scope of this paper.

5. CAVEATS

In this section we make explicit the caveats of our model. We note that our model assumes that all of the injected energy goes into effervescent heating. The amount of energy that is available to effervescent heating, as opposed to the energy that is “lost” to bubble creation, can be estimated from the following simple analytic argument. The available effervescent energy equals the energy lost to bubble expansion as it rises buoyantly, $\int_{P_o}^0 P dV$, where P_o is the pressure at the transition region from the bubble formation region to the buoyant (effervescent) phase. To get the maximum energy available we set the upper limit of the integral to zero pressure. Assuming adiabatic evolution of the gas inside the bubbles (low density, low radiative losses) and mass conservation in the bubble one has $dV = (1/\gamma)(P_o/P)^{1/\gamma} V_o dP/P$, where V_o is the volume of the bubbles at the transition region mentioned above. On integrating, effervescent energy is $3P_o V_o$ for $\gamma = 4/3$ (appropriate to the bubble interior). Thus, since the energy fraction lost to bubble creation at constant pressure

is just $p_o V_o$, approximately only 25% of the injected energy goes to bubble creation, while 75% is available for effervescent heating. We note that if bubble creation occurs at constant pressure, then the injected energy is converted to pdV work on the ICM. The exact details of the dissipation of this energy are as yet unknown, but presumably this process occurs with efficiency lower than 100%. Thus, in the regime where bubble inflation occurs at constant pressure, the above estimate of energy lost to the bubble creation is probably a lower limit. However, if the bubble inflation in the cluster center occurs supersonically, the energy required to inflate the bubble goes into shock heating. Any shocked, high entropy gas is buoyant itself, and acts in a fashion similar to the case described by the effervescent heating function the difference being that a small fraction of the total mass from the innermost radial shells is removed.

We note that our treatment is simplified as we neglect cosmological evolution. In the hierarchical picture, temperature increases with merging as small objects merge to form large objects with higher masses. Also, merging can only increase the entropy. Therefore, heating of the smaller units before they merge, and therefore when they have lower virial temperatures, should reduce the total energy requirement according to the second law of thermodynamics ($dE = TdS$). As clusters observed today ($z \sim 0$) were most likely formed at $z \lesssim 0.5$ (Kitayama & Suto 1996, Balogh, Babul & Patton 1999) and AGN could switch on before the formation epoch of these clusters, lower energy injection could be required to explain observations at $z \sim 0$.

We also note that the hydrodynamics equations have been integrated up to r_{200} . It is likely that the buoyant energy transport would be inhibited by the cluster accretion shock at such large radii. However, excess entropy used to constrain our model is measured at smaller radii and we do not expect this to affect our results significantly.

Our simulations assume that heating is instantaneous. This is an approximation as there should be a delay between the onset of AGN activity and heating at a given radius. We have chosen the shortest heating duration to be at least the sound crossing time (or the dynamical time of rising bubbles) at the outer radius where we compare the computed and observed entropies (r_{500}). Thus, for the shortest heating time, our assumption at $0.1r_{200}$ should be quite reasonable but at r_{500} it would be less accurate but still physically conceivable. For longer heating times our results at both radii should not be affected by this approximation.

Related is the issue of the constraints on the source luminosity. For shorter heating times, higher luminosities are required to assure the same energy injection. Thus, the required luminosities are more feasible for longer heating times. We note also that if the heating is supplied by more than one AGN, then the luminosity requirements on an individual source would be lower. We also reiterate the point made earlier that if the effects of cosmological evolution had been fully taken into account and AGN had supplied heating at earlier epochs, then the energy requirements presented here would have been reduced. Thus, the

source luminosities would also be lower for a given heating time. This is due to the fact that the required excess entropy at higher redshift would be reduced.

6. CONCLUSIONS

We have studied whether “effervescent heating” of cluster gas by a central AGN can resolve the entropy problem in clusters of galaxies. In this model, the AGN (or a group of AGNs in the central region) injects bubbles of buoyant gas, which heat the ICM. The mean volume heating rate due the bubbles is a function of the ambient pressure and a time-averaged energy injection rate to the ICM, but not of the detailed properties of the bubbles or their evolution. We have also included the effects of radiative cooling and convection. We assumed that heating continues for t_{heat} , the duration of heating, and have studied the resulting evolution of the gas assuming it to be in quasi-hydrostatic equilibrium for the Hubble time. The only free parameters of this model are $\langle L \rangle$, the energy injection rate to the ICM, and t_{heat} . The main results of our study are summarized as follows:

1. We find that there are allowed values of $\langle L \rangle$ for which it is possible to match the entropy observations of clusters even at large radii (both $0.1r_{200}$ and r_{500}) with a *single* central AGN for a large range of t_{heat} ($5 \times 10^8 \leq t_{\text{heat}} \leq t_{\text{H}}$ years) and cluster masses ($5 \times 10^{13} - 2 \times 10^{15} M_{\odot}$).
2. Convection plays an important role in removing negative entropy gradients produced by heating in the central regions of the cluster.
3. The results are mostly sensitive to the total energy E_{agn} injected into the cluster by AGN (as cooling effects are relatively mild). The model predicts that the total injected energy $E_{\text{agn}} = \langle L \rangle \times \Delta t$, required to satisfy observational entropy constraints, should be correlated with the cluster mass. This requirement is consistent with a linear relation between the mass of the central black hole(s) and the mass of the cluster, which is reminiscent of the Magorrian relation between the mass of the black hole and the bulge mass of the host galaxy.

We are grateful to the anonymous referee for his/her very constructive comments which helped to improve the paper. We also thank James Binney for sharing with us his views on the details of AGN heating. SR and BBN would like to thank their colleagues in Raman Research Institute for stimulating discussions. MR thanks Phil Armitage for discussions and frequent tea breaks. Support for this work was provided by National Science Foundation grant AST-0307502 and the National Aeronautics and Space Administration through *Chandra* Fellowship Award Number PF3-40029 issued by the *Chandra* X-ray Observatory Center, which is operated by the Smithsonian Astrophysical Observatory for and on behalf of the NASA under contract NAS8-39073.

REFERENCES

- Afshordi, N., & Cen, R. 2002, *ApJ*, 564, 669
- Allen, S.W. et al. 2001, *MNRAS*, 324, 842
- Babul, A., Balogh, M.L., Lewis, G.F., & Poole, G.B. 2002, *MNRAS*, 330, 329
- Balogh, M.L., Babul, A., & Patton, D.R. 1999, *MNRAS*, 307, 463
- Basson, J.F. & Alexander, P. 2003, *MNRAS*, 339, 353
- Binney, J. & Tabor, G. 1995, *MNRAS*, 276, 663
- Begelman, M.C. 2001, in *Gas and Galaxy Evolution*, APS Conf. Proc., vol. 240, ed. Hibbard, J. E., Rupen, M.P., van Gorkom, J.H., p. 363, (astro-ph/0207656)
- Blanton, E.L., Sarazin, C.L., McNamara, B.R., & Wise, M.W. 2001, *ApJ*, 558, 15
- Blanton, E.L., Sarazin, C.L., & McNamara, B.R. 2003, *ApJ*, 585, 227
- Brüggen, M. 2003a, *ApJ*, 593, 700
- Brüggen, M. 2003b, *ApJ*, 592, 839
- Bryan, G.L. 2000, *ApJ*, 544, 1
- Bullock, J.S. et al. 2001, *MNRAS*, 321, 559
- Churazov, E. et al. 2001, *ApJ*, 554, 261
- Clarke, D.A., Norman, M.L., & Fiedler, R.A. 1994, *ZEUS-3D User's Manual Version 3.2.1*, (Urbana-Champaign: Univ. Illinois)
- Davé, R., Katz, N., & Weinberg, D.H. 2002, *ApJ*, 579, 23
- Ettori, S. 2003, *MNRAS*, 344, 13
- Fabian, A.C. et al. 2000, *MNRAS*, 318, 65
- Ferrarese, L., & Merritt, D. 2000, 539, 9
- Finoguenov, A., Reiprich, T.H., & Böhringer, H. 2001, *A&A*, 368, 749
- Gebhardt, K., et al. 2000, *ApJ*, 543, 5
- Häring, N., Rix, H.-W. 2004, *ApJ*, 604, 89
- Heinz, S., Choi Y., Reynolds, C.S., & Begelman M.C. 2002, *ApJ*, 569, 79
- Johnstone, R.M., Allen, S.W., Fabian, A.C., & Sanders, J.S. 2002, *MNRAS*, 336, 299
- Kaiser, C.R., & Binney, J. 2003, *MNRAS*, 338, 837
- Kitayama, T., & Suto, Y. 1996, *ApJ*, 469, 480
- Komatsu, E., & Seljak, U. 2002, *MNRAS*, 336, 1256
- Lloyd-Davies, E.J, Ponman, T.J., Cannon, D.B. 2000, *MNRAS*, 315, 689
- Loken, C., Norman, M.L., Nelson, E., Bryan, G.L., & Motl, P. 2002, *ApJ*, 579, 571
- Mazzotta, P. et al. 2002, *ApJ*, 567, 37
- McNamara, B.R. et al. 2000, *ApJ*, 534, 135
- McNamara, B.R. et al. 2001, *ApJ*, 562, 149
- Muanwong, O., Thomas, P.A., Kay, S.T., & Pearce F.R. 2002, *MNRAS*, 336, 527
- Mushotzky, R. et al. 2003, American Astronomical Society, HEAD meeting, 35, 13.07, astro-ph/0302267
- Nath, B.B. 2003, *MNRAS*, 339, 729
- Nath, B.B., & Roychowdhury, S. 2002, *MNRAS*, 333, 145
- Omma et al. 2003, *MNRAS*, in press, astro-ph/0307471
- Omma & Binney, J., 2004, *MNRAS*, astro-ph/0312658
- Ponman, T.J., Sanderson, A.J.R., & Finoguenov, A. 2003, *MNRAS*, 343, 331
- Peebles, P.J.E. 1980, *The Large Scale Structure of the Universe*. Princeton Univ. Press, Princeton, NJ
- Peterson, J.R., et al. 2001, *A&A*, 365, 104
- Quilis, V., Bower, R.G., & Balogh, M.L. 2001, *MNRAS*, 328, 1091
- Reynolds, C.S., Heinz, S., & Begelman, M.C. 2002, *MNRAS*, 332, 271
- Roychowdhury, S., & Nath, B.B. 2003, *MNRAS*, 346, 199
- Ruszkowski, M., & Begelman, M.C. 2002, *ApJ*, 581, 223
- Ruszkowski, M., Brüggen, M., & Begelman, M.C. 2004, *ApJ*, in press, astro-ph/0310760
- Stone, J.M., Pringle, J.E., & Begelman, M.C. 1999, *MNRAS*, 310, 1002
- Sutherland, R.S., & Dopita, M.A. 1993, *ApJS*, 88, 253
- Tabor, G., & Binney, J. 1993, *MNRAS*, 263, 323
- Tornatore, L., Borgani, S., Springel, V., Matteucci, F., Menci, N., & Murante, G. 2003, *MNRAS*, 342, 1025
- Tozzi, P., & Norman, C. 2001, *ApJ*, 546, 63
- Valageas, P., & Silk, J. 1999, *A&A*, 350, 725
- Voit, G.M., & Bryan, G.L. 2001, *Nature*, 414, 425
- Wu, K.K.S., Nulsen, P.E.J., & Fabian, A.C. 2000, *MNRAS*, 318, 889
- Wu, X., & Xue, Y. 2002, *ApJ*, 572, 19

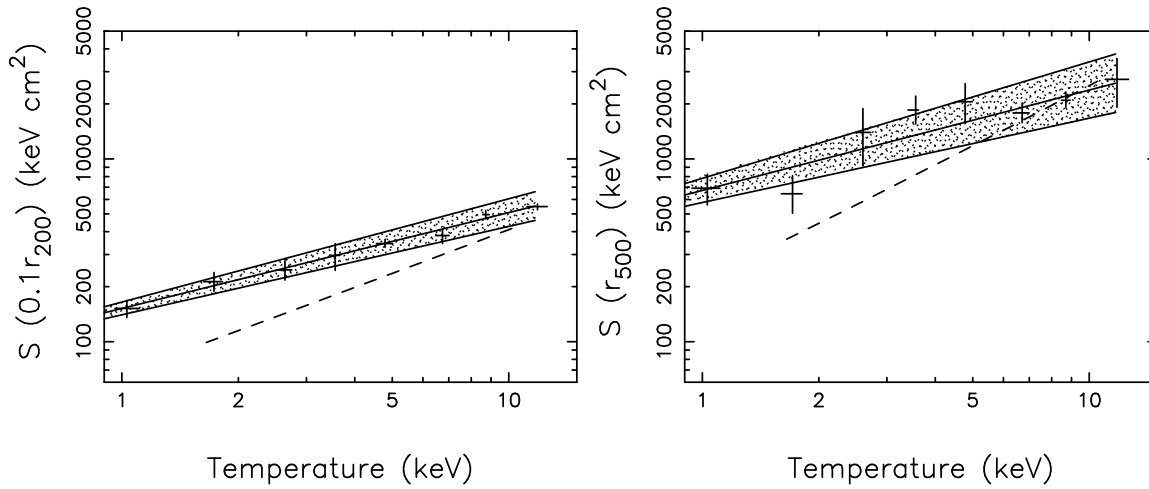


FIG. 1.— Gas entropy (defined here as $T/n_e^{2/3}$) as a function of emission-weighted temperature $\langle T \rangle$, at radii $0.1r_{200}$ (left panel) and r_{500} (right panel). The data points are from Ponman et al. (2003). The solid line in the center of the shaded region is the best-fit to the data points. The two solid lines bounding the shaded region are the $1 - \sigma$ errors on the best-fit values of entropy. The dashed line is the predicted entropy due to gravitational interactions alone (from Roychowdhury & Nath 2003).

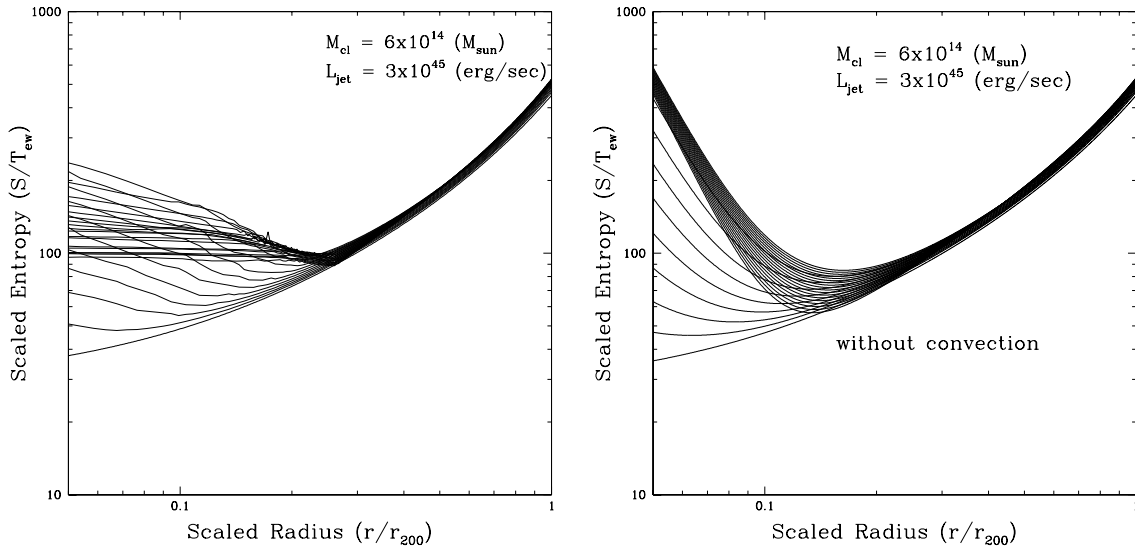


FIG. 2.— Scaled entropy profiles as a function of scaled radius for a cluster of mass $6 \times 10^{14} M_{\odot}$ heated by an AGN with $\langle L \rangle = 3 \times 10^{45} \text{ erg s}^{-1}$, with convection (left panel) and without convection (right panel). The scaled entropy profiles are plotted at intervals of 5×10^8 years. They are seen to rise as the gas is heated and then fall as the gas cools. In both cases $t_{\text{heat}} = 5 \times 10^9$ years. Initial states correspond to the lowest curves.

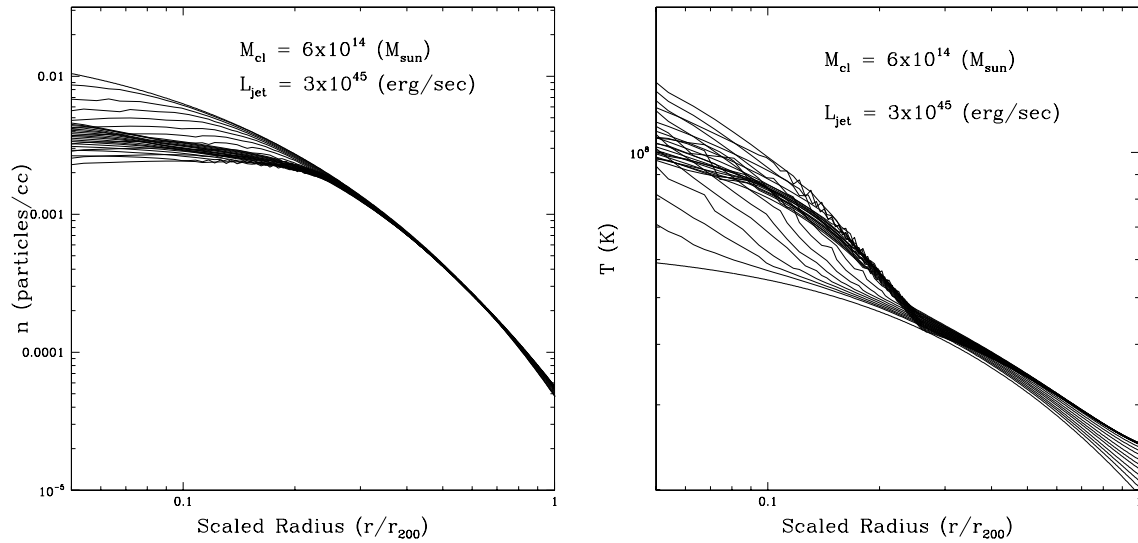


FIG. 3.— Gas density (left panel) and temperature (right panel) profiles as a function of scaled radius (r/r_{200}), for the cluster model shown in the left panel of Figure 2. It is seen here that radiative cooling lowers the temperature, thus increasing the density after the heating source is switched off. Initial density and temperature profiles correspond to the highest and lowest curves, respectively.

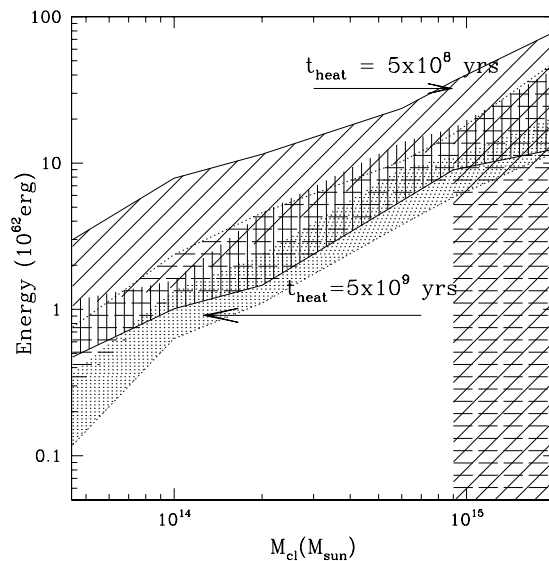


FIG. 4.— Allowed ranges of total injected energy $E_{\text{agn}} = \langle L \rangle \times t_{\text{heat}}$ required to match the observed entropy at $0.1r_{200}$ and/or r_{500} , for two different values of t_{heat} , as a function of cluster mass. The width of each region corresponds to the $1 - \sigma$ errors plotted in Figure 1. The region bounded by thin solid lines corresponds to the allowed range in energies for $t_{\text{heat}} = 5 \times 10^8$ years. Within this bounded region, the area shaded with vertical solid lines is the spread in energy that satisfies the entropy requirement at $0.1r_{200}$ and the area shaded with oblique solid lines is the spread in E_{agn} that satisfies the entropy requirement at r_{500} . Only the overlap region satisfies the observations at both radii. The region bounded by thin dotted lines corresponds to the allowed range in energies for $t_{\text{heat}} = 5 \times 10^9$ years. In this region, the dotted area is the spread in energy that satisfies the entropy requirement at $0.1r_{200}$ and the area shaded with horizontal long-dashed lines is the spread in E_{agn} that satisfies the entropy requirement at r_{500} .

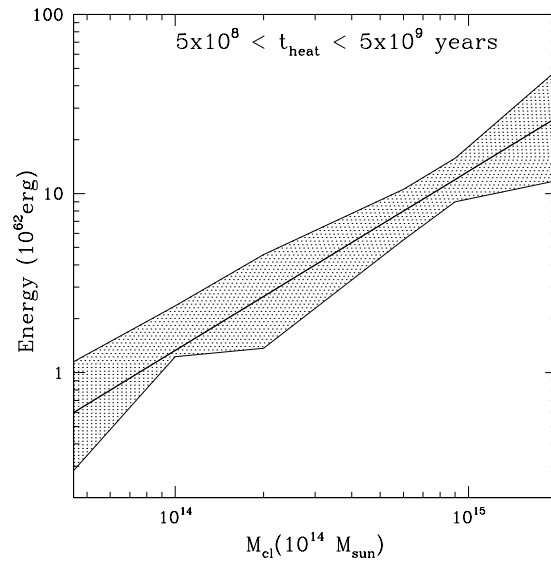


FIG. 5.— This figure shows the permitted total injected energy range as a function of the cluster mass for ICM heating times between $t_{\text{heat}} = 5 \times 10^8 \text{ yr}$ (upper envelope) and $t_{\text{heat}} = 5 \times 10^9 \text{ yr}$ (lower envelope). The shaded region corresponds to values of E_{agn} that are able to match the entropy observations at *both* $0.1r_{200}$ and r_{500} . The thick solid line represents a linear relation between the total energy injected into the cluster by AGN and the mass of the cluster. The permitted parameter space comes from the sum of permitted regions in Figure that satisfy the entropy constraints at both radii for fixed t_{heat} .